Aqueous solvation dynamics with a quantum mechanical Solute: Computer simulation studies of the photoexcited hydrated electron

Benjamin J. Schwartz and Peter J. Rossky
Department of Chemistry and Biochemistry, University of Texas at Austin, Austin, Texas 78712-1167

(Received 2 June 1994; accepted 1 July 1994)

We have used molecular dynamics simulation to explore aqueous solvation dynamics with a realistic quantum mechanical solute, the hydrated electron. The simulations take full account of the quantum charge distribution of the solute coupled to the dielectric and mechanical response of the solvent, providing a molecular-level description of the response of the quantum eigenstates following photoexcitation. The solvent response function is found to be characterized by a 25 fs Gaussian inertial component (40%) and a 250 fs exponential decay (60%). Despite the high sensitivity of the electronic eigenstates to solvent fluctuations and the enormous fractional Stokes' shift following photoexcitation, the solvent response is found to fall within the linear regime. The relaxation of the quantum energy gap due to solvation is shown to play a direct role in the nonradiative decay dynamics of the excited state electron, as well as in the differing relaxation physics observed between electron photoinjection and transient hole-burning (photoexcitation) experiments. A microscopic examination of the solvation response finds that low frequency translational motions of the solvent play an important role in both the inertial and diffusive portions of the relaxation. Much of the local change in solvation structure is associated with a significant change in size and shape of the electron upon excitation. These results are compared in detail both to previous studies of aqueous solvation dynamics and to ultrafast transient spectroscopic work on the hydrated electron.

I. INTRODUCTION

In all of solution phase chemistry, there are few solvents as important as water.[1] With its large dipole moment and strong H bonding, water in particular couples strongly to many chemical reactions, especially those involving the transfer or rearrangement of electrical charge.[2] Indeed, for a wide variety of chemical transformations, the fluctuations of liquid water define the reaction coordinate, determine reaction free energies, and ultimately control aqueous phase reaction dynamics.[2-4] Thus, the nature of the coupling of these fluctuations to the electronic states of solutes is of key importance to the study of aqueous chemical reactivity. This importance is reflected in a number of recent experimental[5-11] and theoretical[12-20] studies exploring the response of aqueous solutions to various types of electrical perturbations, including changes in the dipole moment or charge of a solute and the application of intense optical electric fields.

A unique probe of aqueous solvation dynamics is found in the species of the hydrated electron. Free electrons in the gas phase are described by plane waves: they are completely delocalized, and have no bound states or significant interactions with the radiation field. Electrons in water, however, become self-trapped due to interactions with the solvent.[21,22] The localization of hydrated electrons in the solvent cavity gives rise to bound eigenstates which are modulated by the coupling to aqueous solvent fluctuations. This sensitivity of the electronic states of the hydrated electron to the solvent environment results in an intense, broad electronic absorption which is a direct manifestation of the strong underlying solute–solvent coupling.[20,23] Thus, the hydrated electron serves as a sensitive spectroscopic probe of how aqueous solvent fluctuations couple to electronic species and provides a measure of the solvation dynamics which mediate electron transfer reactions and other chemical transformations.

The purpose of the present paper and that following is to explore the solute–solvent coupling for this model system in detail. In this first paper, we will consider the dynamical response of the solvent and of the solute eigenstates at a molecular level. The second paper analyzes the way in which these molecular features are reflected in spectroscopic observations.

To lay the groundwork for the present study, we first briefly review the spectroscopic features of the hydrated electron and the available experimental probes of these features. Molecular dynamics simulations[20] have found that the lowest energy eigenstate of the hydrated electron is *s*-like in character, filling a nearly spherical solvent cavity about the size of a medium halide ion. The broad absorption band is predominantly accounted for by three transitions to *p*-like excited states (cf. Fig. 1), with smaller contributions from absorptions to higher lying delocalized states in the conduction band comprising the blue spectral tail. The fluctuation broadening by ~0.4 eV of the individual transitions accounts for roughly half the total observed width; the remaining width is due to a splitting of these transitions by a comparable amount.[23]

One way to investigate the solvent contributions to the quantum states comprising the electronic absorption spectrum is the method of transient hole-burning spectroscopy (THB). In THB, an excitation pulse which is spectrally narrow compared to the absorption band of interest is used to excite the subset of solute species which are in local configurations that bring them into resonance with the pulse. Once this subset is promoted to the excited state, an absorption deficit, or spectral hole, is left at the frequency of the excitation pulse; this hole can be measured by a spectrally broad

 0021-9606/94/101(8)/6902/15/$6.00

probe pulse as a function of pump–probe delay time. As time progresses, the initially chosen subset of configurations will be randomized by solvent fluctuations, causing the spectral hole to broaden and leading eventually to a uniform bleaching of the entire band. Barbara and co-workers have performed a series of magic angle (effectively unpolarized) THB experiments on the hydrated electron.[24,25] In these experiments, a three laser pulse sequence is employed. First, a high energy pulse is used to "synthesize" hydrated electrons by multiphoton ionization or negative ion photodetachment. After a several nanosecond delay, equilibrium solvated electrons are photoexcited near the center of the lowest energy absorption subband (indicated on the scale of the calculated spectrum by the position of the arrow in Fig. 1) by a second, near-infrared pulse. Finally, a tunable third pulse, produced by continuum generation, is used to probe the resulting spectral dynamics at a variety of wavelengths. The signal detected in these experiments is the difference in absorption from the equilibrium absorption of the hydrated electron at various time delays after excitation. Due to the finite width of the laser pulses employed and optical dispersion in the sample, the instrumental resolution of these experiments is limited to ~300 fs.[24,25]

In addition to the bleaching of the ground state absorption spectrum, these experiments also measure spectral contributions due to transient excited state absorption and potentially from stimulated emission. Indeed, the experimental traces exhibit a complicated mixture of transient absorption and transient bleaching dynamics over several ps, indicating the importance of these excited state contributions.[24] Traces calculated from molecular dynamics simulations presented in a preliminary report by us,[26] discussed in detail in the following paper, reproduce the observed spectral transients with a high degree of accuracy. The construction of artificial transient signals with various excited state and bleaching contributions removed indicated that evolution of the excited state absorption spectrum combined with ground state bleaching dynamics were responsible for the observed complexity,[26] in contrast to spectral modeling emphasizing the role of solvent cooling around the electron after radiationless relaxation.[25] Thus, aqueous solvation dynamics play a key role in the transient spectroscopy of the hydrated electron.

These THB experiments and simulations are closely related to earlier work probing the relaxation dynamics of electrons injected into neat liquid water.[27–32] Directly following multiphoton ionization, experiments observed a broad absorption peaked in the infrared which decayed in a stepwise fashion into the known equilibrium spectrum of the hydrated electron in a few hundred femtoseconds.[27,28] This behavior was subsequently reproduced by computer simulations,[31,32] which supported the proposed assignment of the infrared absorption to an excited state of the hydrated electron followed by nonadiabatic relaxation to the ground state.[20] A detailed kinetic model of this process has been presented[33,34] which includes the thermalization of the initially delocalized conduction band electrons followed by either trapping of the electron in the lowest excited state and subsequent radiationless transition or direct nonadiabatic relaxation to the ground state.

The spectroscopic differences between the photoinjection[27–30] and THB[24,25] results present some interesting puzzles concerning the nature of the solvent fluctuations coupled to the hydrated electron. In the injection experiments,[27,28] equilibrium solvated electrons are formed very rapidly (within ~0.5 ps), and the presence of an (near)[29] isosbestic point[30] indicates that the equilibrium spectrum is recovered nearly instantaneously upon nonadiabatic relaxation to the ground state, a view supported by adiabatic molecular dynamics simulations.[20] In contrast, the THB experiments[24,25] show spectral transients which persist for several picoseconds and find no evidence for isosbestic spectral behavior. Thus, either the dynamics associated with the excited state, the solvent-induced relaxation to equilibrium upon reaching the ground state, or both must be different between the two cases. Since the photoinjection experiments start with placement of the electron into neat water while the THB experiments photoexcite electrons with the equilibrium solvation structure, the observed differences in relaxation physics must be directly related to differing pathways for solvation dynamics resulting from diverse initial microscopic solvent configurations.

To better understand the connections between aqueous solvation dynamics, microscopic solvent structure, and ultrafast transient spectroscopy, we have performed nonadiabatic quantum molecular dynamics simulations of photoexcited equilibrium hydrated electrons. In what follows, we investigate the solvation dynamics following photoexcitation of the hydrated electron. We explore the details of the aqueous solvent response as it affects the quantum mechanical eigenstates of our hydrated electron probe, and pay special attention to the role of local symmetry and translational modes of the solvent. We compare our solvent response function to previous experimental and theoretical work, and explore the differences in solvent relaxation between the electron injection and photoexcitation experiments. The specific connection between solvation dynamics and the observed ultrafast transient spectroscopy will be discussed in the subsequent paper.

II. METHODOLOGY

In this section, we describe the model system employed to simulate the dynamics of photoexcited equilibrium hydrated electrons. The model system consists of a fully quantum mechanical electron coupled to a bath of 200 classical flexible water molecules. We consider first the model Hamiltonian, then briefly present the algorithm employed for nonadiabatic dynamics, and mention some of the subtleties in the choice of time over which quantum coherence is retained.

A. Electron–water pseudopotential

Since a full quantum mechanical description of the hydrated electron would require an explicit treatment of the excess electron and all the electrons on the water molecules, we have modeled the hydrated electron–water interactions with a pseudopotential. This choice provides an average way in which to treat the interactions between the electrons bound to water and the excess electron while still allowing a quantum mechanical description of the latter. Our choice of

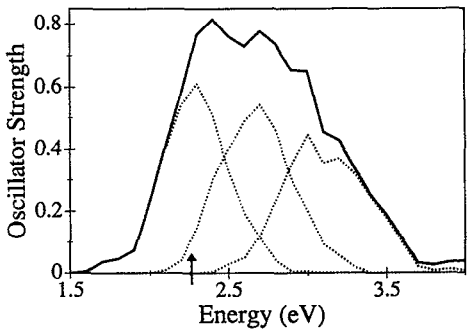

FIG. 1. Equilibrium absorption spectrum of the hydrated electron calculated from ground state adiabatic molecular dynamics simulation (Ref. 31). The dotted lines show the individual absorption components to each of the three p-like excited states. The arrow indicates the energy selected for photoexcitation (2.27 eV) which corresponds (Ref. 58) with the pump laser wavelength used in the experiments of Barbara and co-workers (Refs. 24 and 25).

pseudopotential[35] is based on both its sound theoretical justification and the ease of comparison to previous quantum simulations.[20–23,26,31,32,36–38] This pseudopotential consists of a sum of several terms, representing the Coulomb interactions between the excess electron and the partial charges on the hydrogen and oxygen atoms of the solvent molecules, the polarization interaction between the water molecules and the hydrated electron, and the orthogonality requirement between the wave function of the excess electron and solvent molecular wave functions (Pauli exclusion principle). A detailed discussion of this potential is available in Ref. 35.

The calculated optical absorption spectrum of the hydrated electron which follows from this model, presented in Fig. 1, reproduces the intensity, shape, and width of the experimental spectrum quite well, although the calculated[23,31] peak frequency is blueshifted from experiment.[39,40] Previous simulations employing this pseudopotential have also captured the correct microscopic physics of the hydrated electron, as evidenced by the excellent agreement between calculated[26,31,32] ultrafast spectroscopic transients and those measured in both electron injection[27,28] and transient hole-burning[24,25] experiments.

B. Water–water interactions

One of the chief advantages of computer simulation is that it allows for description of the solvent at the molecular level. For water in particular, there are many well-characterized models from which to choose. Recent work exploring the model dependence on the properties of the hydrated electron[31] has led us to select a flexible version of the simple point charge model (SPC flexible) due to Toukan and Rahman.[41] In this model, intramolecular flexibility is simply added onto the well-known SPC intermolecular potential,[42] which consists of Lennard-Jones interactions centered on the oxygen atoms plus Coulomb interactions between partial charges located on the different atomic sites. The properties of this model for water have been explored in detail and have been compared both to other models and to experiment.[41,43–45]

It is important to note that the use of a classical model for water is expected to affect the overall time scale of the computed relaxation dynamics. As has been pointed out previously,[26,31] the oscillators in classical flexible water can accept any amount of energy from the relaxing electron, providing for potentially faster energy disposal than real water in which energy acceptance is quantized. This is likely the cause of nonadiabatic relaxation dynamics in earlier simulations[26,31] which appear to be approximately a factor of 2 faster than those measured by experiment. Thus, while the solvation response should be well described by this model of water, the excited state lifetime presented here for the hydrated electron would be expected to somewhat shorter than that observed experimentally.

C. Algorithm for nonadiabatic dynamics

Whenever the dynamics of a condensed phase system are coupled strongly to a quantum solute, movement of the solvent atoms can lead to nonradiative excitation or relaxation of the quantum subsystem.[46] Such nonadiabatic transitions, corresponding to a breakdown of the Born–Oppenheimer approximation, become especially important when the difference between energy levels of the quantum solute is comparable to the energy of nuclear motion of the solvent. Restricting the hydrated electron to a single potential energy surface with purely adiabatic techniques cannot adequately reproduce the observed relaxation dynamics or transient spectroscopy.[20,32] Thus, we employ an algorithm including state-to-state transitions; quantum coherence is treated explicitly during the propagation of mixed quantum states, and a prescription for nuclear dynamics is included that conserves energy and angular momentum during nonadiabatic transitions between eigenstates.

The algorithm for nonadiabatic dynamics we use, developed by Webster and co-workers,[32,47,48] is based on a combination of the stochastic surface hopping approach of Tully and Preston[49] and the nonadiabatic scattering formalism of Pechukas.[50] Briefly, the algorithm works as follows: the solvent coordinates at time t_0, $\mathbf{R}(t_0)$, define an electronic Hamiltonian for the quantum subsystem via the pseudopotential described above. The set of adiabatic eigenstates for the solute, $\{\alpha(t_0)\}$, can be determined by solving the time-independent Schrödinger equation for this solvent configuration. When the system is propagated forward to time t under the influence of both the classical and quantum forces, a new set of adiabatic eigenstates, $\{\beta(t)\}$, can be determined. As propagation of a pure initial state $\alpha(t_0)$ will, in general, produce a mixed quantum final state at time t, we use stochastic surface hopping to determine the new occupied adiabatic eigenstate. Writing the quantum propagator as $U(t,t_0)$, the transition amplitudes between the initial and final adiabatic eigenstates are defined as

$$T_{\beta\alpha}=\langle\beta(t)|U(t,t_0)|\alpha(t_0)\rangle. \tag{1}$$

The squares of the transition amplitudes, which are the overlap between the propagated initial state and the possible final states, determine the probability for transition to each final adiabatic state. The new state is chosen by comparing these squared amplitudes to a random number (stochastic surface

hopping). If the chosen state on the new step differs from the occupied state on the previous step, a nonadiabatic transition is made. Once a final state is selected, the force that the quantum system (in its mixed state) exerts on the classical coordinates is given by

$$F_Q(t) = -\mathrm{Re}[\langle\beta(t)|U(t',t)\nabla_{\mathbf{R}}V[\mathbf{R}(t)] \times U(t,t_0)|\alpha(t_0)\rangle]/T_{\beta\alpha}. \quad (2)$$

This expression for the quantum force,[50] derived using the stationary phase approximation for the nuclear coordinates in a path integral representation of the quantum propagator, is nonlocal in time: the force depends on the nuclear configuration throughout the propagation. In practice,[47] an initial guess based on a linearized Hamiltonian is used to calculate approximate nuclear dynamics, resulting in a better guess at the quantum force, and the process repeated until self-consistency is achieved.

In the present application of the nonadiabatic algorithm outlined above, we choose to drop the quantum coherence at the end of each time step when the new adiabatic eigenstate is selected. An alternative nonadiabatic dynamic algorithm,[51,52] based on Tully's approach,[53] includes retention of quantum coherence over an arbitrarily long time. Our choice can be justified in part by a recent result of Neria *et al.*,[54,55] who computed the nonadiabatic transition rate for the excited hydrated electron with a formalism based on the golden rule using a semiclassical treatment of the solvent. These calculations indicate that quantum coherence following a transition of the hydrated electron decays in only a few fs, apparently predominantly due to dephasing of the *nuclear* wave function of the solvent. Thus, for the photoexcitation of the hydrated electron to its first excited state, we favor the method outlined above and choose a coherence time equal to the 1 fs simulation time step. A recently developed nonadiabatic algorithm which combines the Pechukas expression Tully's approach shows promise for future simulations.[56]

D. Computational details

The model system is described by a cubic cell of side 18.17 Å containing 200 classical flexible SPC water molecules (solvent density of 0.997 g/ml) and one quantum mechanical electron. The system temperature was 300 K. Standard periodic boundary conditions were employed, and all interactions were evaluated with a smooth spherical cutoff terminating at a distance of 8.0 Å as in earlier work.[31] The adiabatic eigenstates at each time step were obtained via an efficient iterative and block Lanczos scheme[47] using a 16^3 plane wave basis; the lowest 6 eigenstates were computed during nonadiabatic dynamics. The equations of motion were integrated using the Verlet algorithm[57] and a time step of 1 fs.

The starting point of the simulations was obtained by first injecting an excess electron into neat water and equilibrating the resulting ground state electron for 15 ps. After equilibration, a 35 ps (adiabatic) ground state trajectory was calculated and divided into 20 equal parts, and the first configuration in each segment which was resonant with the pump laser (2.27 ± 0.01 eV corresponding[58] for the model Hamiltonian to an experimental pump pulse centered at 780 nm with a ~ 200 cm^{-1} bandwidth, shown by the arrow in Fig. 1) was chosen as a starting point for one of the 20 excited state trajectories considered here. Of the 20 excited state trajectories, 16 were launched on the first excited state while 4 were found to be promoted to the second, corresponding to the ratio expected given the intensities of the subbands to the different p-like states at the wavelength of the laser evident in Fig. 1. During propagation on the excited state, attempted nonadiabatic transitions to the ground state were rejected if $|T_{\alpha\beta}|^2 < 0.001$ and energy was not conserved after 5 self-consistent iterations. All remaining transition attempts were accepted, with typical transition amplitudes $10^{-3} \leqslant |T_{\alpha\beta}|^2 \leqslant 10^{-2}$, and the energy of the entire system was conserved to better than $\pm 0.2\%$ at all times.

III. RESULTS

In this section, we present the results of our nonadiabatic quantum simulations of the photoexcitation of equilibrium aqueous solvated electrons. We first discuss the characteristics of individual trajectories, and comment on the similarities and differences compared to those observed in earlier studies of electron injection.[31,32] Next, we will use ensemble averaged kinetics to explore the nature of the aqueous solvation dynamics following both the photoexcitation and the nonadiabatic return to the ground state. The time evolution of the energy gap is found to play an important role in the dynamics of the radiationless transition, and we compare our results to those of other calculations and to experiment.

A. Nonadiabatic trajectories

For any given instantaneous configuration of the solvent, there exists a well-defined set of adiabatic eigenstates for the aqueous solvated electron. As the solvent configuration evolves with time, coupling to the quantum solute will cause the adiabatic eigenstates to fluctuate. Size fluctuations of the solvent cavity containing the electron modulate the magnitude of the energy gaps between the ground and first 3 excited states, and cavity shape changes correlate with the splitting between the excited states.[20,36,37] By following the dynamics of these energy levels both at equilibrium and upon photoexcitation, we can gain a great deal of insight into the physics underlying photoexcitation of hydrated electrons as well as learning more about the nature of aqueous solvation dynamics.

Figures 2 and 3 present representative paths through state space for the hydrated electron for 2 of the 20 trajectories. The solid and dashed lines denote the dynamical history of the adiabatic eigenstates, while the small diamonds mark the occupied state. Figure 2 displays behavior which is typical for most of the runs. Before the excitation (negative times), we see a portion of a typical ground state trajectory for the hydrated electron. The s-like ground state is bound by roughly 2.5 eV, and the p-like excited states, split by ~ 0.5 eV, are readily observed as the next three states near the vacuum level. Two of the delocalized states in the continuum band which lie just above the three p-like states are shown for completeness. The energy levels are modulated strongly by solvent motions, but the three states do not interchange

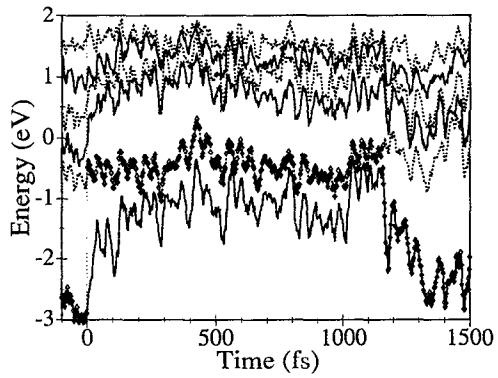

FIG. 2. Dynamical history of the adiabatic eigenstates for a typical trajectory describing electron photoexcitation. Alternating solid and dashed lines denote the adiabatic eigenstates, the small diamonds denote the occupied eigenstate. The electron is promoted from the equilibrium ground state into the first excited state at $t=0$.

roles during the brief interval shown, corresponding to the fact that the orientation of the solvent cavity is not changing significantly on this short time scale.[37]

At $t=0$, the energy gap between the ground and lowest excited states becomes resonant with the laser, and the electron is promoted to the first excited state. As the solvent responds to the change in electronic charge distribution, the energy of the newly occupied excited state stays relatively constant, but marked changes take place in the energies of the other adiabatic eigenstates. The energy of the now unoccupied ground state shoots up very quickly, and then continues to rise and approach the energy of the occupied state at longer times. The upper two p-like states also rapidly increase in energy, creating a fair-sized gap between the occupied state and higher lying excitations. For this run, roughly 1140 fs after the excitation, the electron undergoes a radiationless transition, crossing the roughly 0.4 eV gap between the occupied and ground states. The adiabatic eigenstates reverse their behavior after excitation and quickly return to equilibrium. The ground state energy drops precipitously until it is bound by ~2.5 eV, and the upper two p states drop down to reform the band consisting of the first 3 excited states.

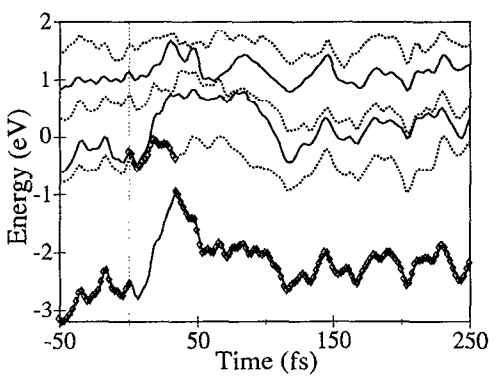

FIG. 3. Dynamical history of the adiabatic eigenstates for one of the four trajectories in which the electron was promoted into the second excited state. Coincidentally, this trajectory also had the shortest excited state residence time. Symbols are the same as in Fig. 2.

The trajectory shown in Fig. 3 is slightly unusual in two respects: it is one of the four trajectories that was promoted to the second excited state upon excitation, and it is also has the shortest excited state residence time of all the trajectories, undergoing the radiationless transition in only 35 fs. Before the excitation, the lowest 2 p-like states are fairly close in energy, while the third p-like state lies significantly higher, indicating that the solvent cavity in these configurations is significantly narrower in one direction than in the other two. At $t=0$, the gap between the ground and second excited states met the resonance condition, and the electron was promoted into the second excited state. Within 15 fs, the first and second excited states cross, leaving the electron occupying the lowest excited state. After the nonadiabatic transition at 35 fs, the ground state rapidly drops back toward its equilibrium value, and the excited states follow suit within another 50 fs. This phenomenon, the rapid return to equilibrium after nonadiabatic relaxation, appears to be general across all 20 trajectories, and is consistent with older adiabatic results.[20]

It is interesting to compare the results of Figs. 2 and 3 to the work of Space and Coker simulating the quantum dynamics of an excess electron in liquid helium.[51,52] Like the hydrated electron, the excess electron in helium exhibits a trapped, s-like ground state. Excitation into the second p-like state of the electron in helium exhibits similar characteristics to the behavior seen here in Fig. 3. There is a very rapid diabatic interchange with the first excited state, after which the electron remains trapped in the first excited state for a longer period before undergoing radiationless transition to the ground state. After nonadiabatic relaxation, equilibrium is established quickly for both electrons in helium and water. The helium simulations, however, show that most of the solvent relaxation acts to lower the energy of the first excited state rather than raising the energy of the ground state as seen in Figs. 2 and 3. This is likely related to the very different electron–solvent interactions and corresponding structure of the electron between the two fluids. As discussed below, the equilibrium excited state hydrated electron is much larger than the ground state hydrated electron, while the excess electron in liquid He remains roughly the same size in both the ground and excited states.[51]

The trajectories presented in Figs. 2 and 3 also show two principal contrasts to those calculated with this same model for electron injection into neat water.[31] First, the injection simulations found two qualitatively different types of trajectories: those that cascaded quickly to the ground state and those that were trapped for some period of time in the lowest excited state. All of the trajectories run here, including that presented in Fig. 3, show qualitatively similar behavior. Second, the average excited state residence times for photoexcited electrons are ~5 times longer than for electrons trapped in the excited state following photoinjection calculated with the same model and algorithm.[31] This result is in qualitative agreement with experiment: spectral transients after electron injection show no changes due to solvation after ~500

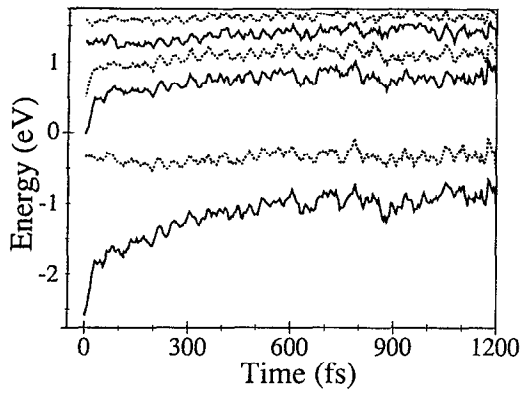

FIG. 4. Ensemble averaged adiabatic eigenstates (alternating solid and dashed lines) for configurations in which the electron occupies the first excited state, demonstrating the effects of solvation dynamics on the quantum energy levels. As trajectories undergo nonadiabatic relaxation to the ground state they are removed from the average, leading to poorer statistics at longer delay times.

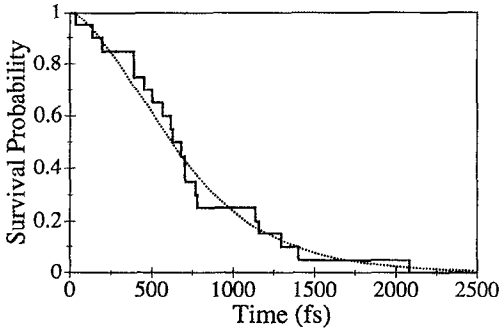

FIG. 5. Excited state survival probability as a function of time. The solid curve denotes the fraction of trajectories in which the electron still resides in the excited state. The dashed curve is a fit to a simple one-parameter model described in the text which assumes an inverse linear proportionality between the quantum energy gap and the nonadiabatic transition rate.

fs,[27-30] whereas spectral dynamics after photoexcitation of equilibrium electrons persist for several ps after excitation.[24,25] Clearly, the physics of electron solvation after injection are different from those produced by photoexcitation.

B. Solvent response to perturbation

To better understand the observed behavior of the hydrated electron after photoexcitation, we have computed the ensemble average of the adiabatic eigenvalues after photoexcitation including only configurations in which the excited state is still occupied. This result is shown in Fig. 4. At early times, the electron occupies the excited state in all 20 trajectories, giving good statistics and low apparent noise. As time progresses, an increasing number of electrons undergo the radiationless transition and are removed from the ensemble. By 1200 fs, the average contains contributions from only 5 trajectories, resulting in significantly poorer statistics. Figure 4 clearly shows the effects of solvation dynamics on the adiabatic eigenstates following the electrical and mechanical (i.e., the short range repulsive forces due to the Pauli exclusion principle) perturbations which occur upon photoexcitation.

Once photoexcited, the energy of the ground state shows a rapid relaxation on a ~25 fs time scale, followed by a slower evolution over a few hundred fs. The energy of the occupied excited state undergoes little change: the solvent response to the potential energy of the new charge distribution is canceled by the resultant change in the electron's kinetic energy. These results are in good agreement with the adiabatic excited state molecular dynamics simulations of Barnett *et al.*[18] in water clusters. Figure 4 also shows the effects of solvation on the upper two p states, which like the ground state, show a rapid initial increase in energy followed by relaxation over a longer time scale. The higher energy delocalized states do not exhibit a rapid solvation response, but do appear to drift slightly upwards in energy over a several hundred fs time scale following promotion to the excited state. For times $\geqslant$500 fs, the equilibrium excited state is characterized by an average 0.56 eV energy gap to the ground state and by a $\approx$1 eV energy difference to the next higher lying state.

The final point to note from the results of Figs. 2–4 is the extremely strong coupling of the electronic eigenstates to aqueous solvent fluctuations. The energy levels of the hydrated electron fluctuate by nearly an eV (thousands of wave numbers) on time scales of tens of femtoseconds (Figs. 2 and 3), making the electron an especially sensitive probe of aqueous solvation dynamics. This strong coupling can also been seen in the enormous Stokes' shift of the quantum energy gap following excitation: the average energy gap relaxes by about 75% of the initial excitation energy, from 2.27 to 0.56 eV (Fig. 4). This represents what is probably the largest fractional Stokes' shift for any solute; the strength of this coupling is one of the key features which makes the solvated electron an outstanding spectroscopic probe of solvation dynamics.

C. Survival probability of the excited state

Because the solvent-induced fluctuations of the energy levels of the hydrated electron are comparable to the spacing between them, it is essential to use a nonadiabatic description for the electronic dynamics. The 20 trajectories launched here show a wide range of nonadiabatic transition times; consideration of the entire swarm of trajectories provides valuable information about the overall nonadiabatic relaxation rate for excited hydrated electrons.[32,47,54,55] The solid line in Fig. 5 presents the occupation probability of the excited state for the entire set of trajectories. For example, at 35 fs, the shortest trajectory (Fig. 3) undergoes nonadiabatic relaxation, leaving 19 out of 20 runs still in the excited state, causing the survival probability to jump to 0.95. At times past 2.1 ps, the electron occupies the excited state in none of the 20 trajectories, resulting in a survival probability of zero.

The survival probability distribution yields an average lifetime of 730 fs and a median nonadiabatic transition time of 630 fs, but perhaps the most striking feature of Fig. 5 is the marked nonexponential behavior of the population decay.

Even given the statistical noise inherent in the relatively small number of examples (if the survival probability obeys Poissonian statistics, the relative error in Fig. 5 should be about $\sqrt{20}/20 \approx 0.2$), the excited state relaxation is clearly nonexponential for times ≤ 500 fs; the population decays much too slowly and the curvature is opposite to that described by an exponential decay. This phenomenon is a reflection of the excited state solvation dynamics which modulates the energy gap after photoexcitation, as seen in Fig. 4. If the probability of nonadiabatic relaxation increases with a decrease in the energy difference between the occupied and ground states, then the radiationless transition rate will be significantly slower at early times when the gap is large. Once the solvation response is complete and the average gap energy is no longer changing with time, the nonadiabatic relaxation dynamics should proceed exponentially. Thus, the shape of the survival curve is dictated strongly by solvation dynamics.

The dashed line in Fig. 5 is given by a simple model based on an analytical fit to the dynamical energy gap, which is discussed in more detail in the next section after analysis of the solvation dynamics. For times ≥ 500 fs, a constant nonradiative lifetime of the equilibrium excited state appears valid. In this region, the dashed line corresponds to the best fit with an equilibrium nonadiabatic transition rate of $(450\ \text{fs})^{-1}$.

This equilibrium excited state lifetime can be compared to the recent semiclassical calculations of Neria and Nitzan,[54,55] in which frozen Gaussians were used to describe the solvent nuclear contribution to the total wave function in an expression based on the golden rule. Based on the results of 15 trajectories of 10 fs each, a nonradiative lifetime of 220 fs for the excited state of the electron in H_2O was estimated.[55] Neria and Nitzan[55] note that their calculated lifetime is subject to considerable numerical uncertainty. Considering this fact, the agreement of this estimate with the equilibrium lifetime calculated from our simulations, which used a different model, seems satisfactory.

In comparing this lifetime to experiment, it is important to note that the spectroscopic experiments of Long *et al.*[28] and Gauduel *et al.*[27] (leading to excited state lifetime estimates of 540 and 240 fs, respectively) measure relaxation dynamics after electron injection, and hence never probe the electron in its equilibrium excited state. A more appropriate comparison would be to the more recent photoexcitation experiments of Barbara and co-workers,[24,25] in which the electron resides in the equilibrated excited state after the solvent response is complete. The long-lived spectral transients indicate a reasonably slow relaxation rate for the equilibrium excited state hydrated electron.[26] While the assignment of the spectral transients in the photoexcitation experiments will be discussed in more detail in the following paper, it is clear that the relaxation dynamics after injection are much more rapid than those following photoexcitation. As pointed out above, we expect the nonradiative lifetime calculated here to be smaller than experiment.

IV. THE HYDRATED ELECTRON AS A PROBE OF AQUEOUS SOLVATION DYNAMICS

In this section, we investigate aqueous solvation dynamics as manifest through coupling to the quantum states of the hydrated electron, and compare to previous calculations and experiments exploring the electrical solvent response of water. We analyze the microscopic features of the solvation structure and examine the physics underlying the aqueous solvent response.

A. Solvent fluctuations coupled to the aqueous solvated electron

The effects of solvent fluctuations on the energy gap of a quantum solute are described by the equilibrium solvent response function:

$$C(t) = \frac{\langle \delta U(0)\, \delta U(t) \rangle}{\langle (\delta U)^2 \rangle}, \tag{3}$$

where $U(t)$ is the value of the quantum energy gap at time t and $\delta U(t) = U(t) - \langle U \rangle$ represents the fluctuation of the gap from its equilibrium average value.[2,3] In the limit of linear response, the regression of fluctuations resulting from a perturbation should decay in the same manner as those present at equilibrium. Thus, for small perturbations, Eq. (3) is equivalent to the nonequilibrium response function

$$S(t) = \frac{\langle U(t) \rangle_{ne} - \langle U(\infty) \rangle_{ne}}{\langle U(0) \rangle_{ne} - \langle U(\infty) \rangle_{ne}}, \tag{4}$$

where the subscript "ne" denotes a nonequilibrium ensemble average. In experiments, the nonequilibrium response function $S(t)$ is typically measured by the time-dependent Stokes' shift of fluorescence following the electric dipole change upon excitation of a dye molecule,[2,3,9–11,59] or more recently, by transient alignment of the neat solvent with the applied electric field of an ultrafast laser pulse via the optical Kerr effect.[5–8,60]

The hydrated electron provides a unique probe of the coupling of aqueous solvent fluctuations to the quantum electronic states of solutes. Simulations of aqueous solvation dynamics have to this point (with a few exceptions)[15–18] relied on calculating the electrical potential produced by the solvent at the solute as an approximation to obtain the change in the quantum energy gap, and many employ classical electrostatic point charge models to compute the energy. With the quantum technique we employ, these approximations are avoided as we treat the full wave function of the electron explicitly and directly examine the response of the quantum eigenstates to solvation. The principle drawback to the use of the hydrated electron as a probe of aqueous solvation dynamics lies in its short excited state residence time: solvent response on time scales longer than the radiationless lifetime will not be observed.

Figure 6 presents the nonequilibrium solvent response function [Eq. (4)] for photoexcitation of the hydrated electron. This response is essentially the energy gap following promotion into the excited state seen in Fig. 4, but normalized to start at 1 and decay to zero. While the initial excitation energy $\langle U(0) \rangle_{ne}$ is well defined by the resonance con-

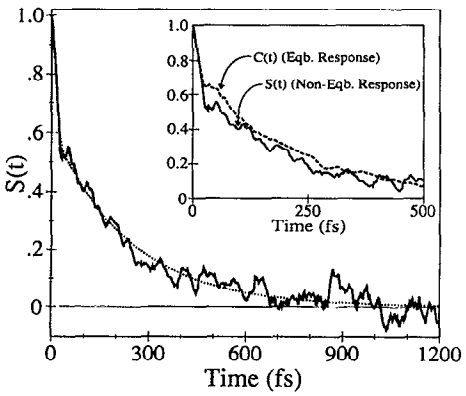

FIG. 6. Nonequilibrium solvent response function following photoexcitation of the hydrated electron computed from Eq. (4). The relationship to the lowest quantum energy gap seen in Fig. 4 is discussed in the text. The dotted line shows a fit to a 25 fs Gaussian+240 fs exponential decay. The inset compares the equilibrium energy gap autocorrelation [Eq. (3)] to the nonequilibrium response function; the good agreement indicates that the solvation dynamics fall within the linear response regime.

dition, the finite excited state lifetime leads to some ambiguity as to the choice of a value for $\langle U(\infty)\rangle_{ne}$ in the use of Eq. (4). As it appears that the solvent response is well over by a time delay of 1 ps, we have used an average of the excited state configurations past 1 ps to determine the 0.56 eV asymptotic value of the average energy gap. Like the ensemble average used in Fig. 4, the statistics used in the calculation of $S(t)$ become poorer at longer time delays. The solvation response presented in Fig. 6 shows two main components: an ultrafast response causing rapid decay within the first 30 fs, and a slower response which takes place over a time scale of several hundred fs. The fast portion of the decay is due to the "inertial" solvent response, also referred to as "ballistic motion" or "molecular free streaming."[2,61] This type of rapid Gaussian inertial response has been predicted by theory,[19,62–64] observed in many simulations[2,12–20,61] and more recently, measured by experiment.[11,65–67] The dotted line in Fig. 6 represents a Gaussian+exponential fit to $S(t)$. The inertial portion of the response fits well to a 24 fs Gaussian with an amplitude of 38%, and the remaining 62% of the response is well described by a 240 fs decaying exponential.

The time scales for the aqueous solvent response function presented here agree well with those found in previous simulations and experiment. The strong similarity with the hydrated electron work of Barnett *et al.*[18] was mentioned in the previous section. Using an experimentally determined dielectric dissipative kernel in a molecular hydrodynamic theory, Roy and Bagchi[19] calculated a solvent response function for water with a ~20 fs Gaussian inertial decay followed by exponential relaxation with time constants of 250 fs and 1 ps. Maroncelli and Fleming[12] used the ST2 model of water and a variety of simple ionic solutes to simulate aqueous solvation dynamics, and found a rapid ~25 fs inertial component and a slower, ~200 fs exponential relaxation. Jarzeba *et al.*[9] experimentally measured the dynamic Stokes' shift of Coumarin dye molecule in water and obtained a biexponential solvent response with time constants 0.16 and 1.2 ps. In this case, the 280 fs instrument function of the fluorescence upconversion apparatus employed prevented observation of the fast Gaussian component and accurate determination of the more rapid decay time. The Raman-induced Kerr effect recently employed by Chang and Castner[5,6] measured similar responses of water on 0.4 and 1.2 ps time scales. As mentioned above, the short excited state residence time of the hydrated electron makes it a poor probe of solvation dynamics on the ps time scale, but our calculated 24 fs Gaussian and 240 fs decays agree well with all the previous work. However, the longer relaxation on the ~1 ps time scale does appear in calculated hole-burning dynamics, as will be discussed further in the subsequent paper. Finally, we note that the ~240 fs time observed in all these works is roughly equal to the longitudinal relaxation time (τ_L) for liquid water.

One notable difference between the solvent response function presented in Fig. 6 and some of those presented elsewhere lies in the relative amplitude of the inertial component. Theoretical work relating the solvent response to the neat liquid dipole autocorrelation function,[68] along with the simulations by Maroncelli and Fleming[12] indicate that the inertial component accounts for 80%–90% of the total aqueous solvent response, in contrast to the ~40% observed here. One possible explanation for this discrepancy lies in the different models used for water in the two simulations. In their molecular hydrodynamic theory, Roy and Bagchi found that the inclusion of polarizability made a large difference in the initial solvent response: with experimentally determined (and hence, polarizable) dielectric parameters for water, their computed inertial amplitude was ~65%, whereas dielectric parameters chosen to mimic the rigid ST2 model employed by Maroncelli and Fleming resulted in a ~85% inertial response.[19] Since the water model used in our simulations is somewhat polarizable due to the internal flexibility, this could explain part of the differences between our results and those of Maroncelli and Fleming. Our results are in reasonable agreement with the ~50% inertial component observed by Barnett *et al.* for the excited hydrated electron in flexible RWK2-M water clusters.[18] Another possibility lies in the multipolar nature of the change in charge distribution of the electron upon photoexcitation. Recent work by Kumar and Maroncelli[69] has shown that the relative amplitude of the inertial component of the solvation response is inversely related to the multipole order of the change in charge distribution. For the electron, in a multipole expansion for the $s\rightarrow p$ like transition, the monopole term is zero since the charge does not change and the dipole term should be small (since in an idealized $s\rightarrow p$ transition it would also be zero), possibly explaining the smaller inertial response.

There is an important additional novel feature of the present system that is also a likely contributor to the relatively small amplitude of the inertial portion of the solvation response. The fact that the solute changes size and shape (and hence, charge distribution) during the solvation response is something that has not been typically accounted for in previous simulation and theoretical studies. Notable exceptions lie in the work of Levy *et al.*[15] and Muiño &

Callas,[16] who represented the electrical potential of their solutes (such as formaldehyde or indole) by point charges determined from *ab initio* calculations performed at each solvent configuration. The solvent responses to these solutes are qualitatively similar to that presented in Fig. 6 for the solvated electron. Another possibility for explaining this discrepancy lies in the large change in size of the electron upon excitation which might couple the electrical and mechanical responses of the solvent, as will be discussed in more detail below.

We now consider the question of linearity in the solvent response. The inset of Fig. 6 shows an expanded view of the first 500 fs of the solvent response function, and compares it to the equilibrium solvent response calculated from ground state dynamics via Eq. (3). The nonequilibrium $S(t)$ agrees well with the equilibrium response, indicating that photoexcitation of the solvated electron falls within the linear response regime. This same nonequilibrium response function can also be computed in another way, from the time-dependent Stokes' shift of the emission spectrum.[2,3,59] As will be discussed in more detail elsewhere,[70] we have used the method of spectral reconstruction[2,3] to compute $S(t)$ from the simulated emission data and find excellent agreement with the directly determined response functions presented in Fig. 6.

It is also interesting to note that the absolute magnitude of the solvent response also falls within the linear regime. In the linear response limit, the mean square amplitude of the solvent fluctuations of the quantum energy gap, $\langle \Delta\omega^2 \rangle$, is related to the magnitude of the Stokes' shift, 2λ, by the fluctuation-dissipation theorem[71]

$$\langle \Delta\omega^2 \rangle = 2\lambda k_B T. \tag{5}$$

From the standard deviation of the fluctuations of the quantum energy gap about equilibrium, we obtain a value for $\langle \Delta\omega^2 \rangle^{1/2}$ of $\sim 1700\ \mathrm{cm}^{-1}$. At room temperature, this gives a predicted Stokes' shift from Eq. (5) of $\sim 14\,300\ \mathrm{cm}^{-1}$, in good agreement with the observed nonequilibrium Stokes' shift of $\sim 13\,800\ \mathrm{cm}^{-1}$ (1.71 eV) seen in Fig. 4.

Finally, the analytic fit to the time dependence of the energy gap following photoexcitation can be used to estimate the nonradiative lifetime of the equilibrium excited state. Noting that the equilibrium value of the energy gap, 0.56 eV, is roughly 33% of the total solvation response (which decreases the gap by $2.27-0.56=1.71$ eV), and using the analytic fit to $S(t)$ shown in Fig. 6, we can write the time-dependent gap change, normalized to the size of the equilibrium gap after completion of the solvation response, as: $U(t)=0.76\ \exp[-\frac{1}{2}(t/24)^2]+1.24\ \exp(-t/240)+1$ for t in fs. To use this result, we need a relationship between the energy gap and the transition rate. An ansatz that works is one with a relatively weak dependence. If we assume that the probability of nonadiabatic decay is inversely proportional to the magnitude of the gap, then population of the excited state is described by

$$\frac{dP(t)}{dt} = \frac{-P(t)}{\tau U(t)}; \quad P(0)=1, \tag{6}$$

where $P(t)$ is the population in the excited state at time t after excitation and the proportionality factor τ is simply the excited state lifetime after the gap has reached its equilibrium value. Equation (6) can be solved analytically for $P(t)$, leaving τ as the only undetermined parameter. A nonlinear least squares fit of $P(t)$ to the simulated survival probability, shown in Fig. 5 as the dashed line, gives a best value for τ of 450 fs.

Although the fit in Fig. 5 is not perfect and the data include uncertainty, the fit does reproduce the negative curvature at early times, and matches the inflection point which occurs near 700 fs. This indicates that the nonadiabatic transition probably does depend more or less inversely on the energy gap, as in our ansatz. The negative curvature at early times can be explained by this dependence. At $t=0$, the gap is quite large, so the transition probability is low and the population tends to remain in the excited state. As time progresses, the gap decreases, leading to an increasing population decay rate with time. Finally, the decay rate levels off to its maximum value as the gap approaches equilibrium, resulting in an exponentially decreasing probability with time. Thus, although we presently have no *a priori* justification, our simple model captures the qualitative physics underlying the population decay, and provides a reasonable estimate of the equilibrium excited state lifetime.

The energy gap dependent radiationless transition rate can also be used to explain some of the differences in time scale observed between electron injection and photoexcitation. In the injection case,[31,32] the eigenstates of the hydrated electron in neat water are highly delocalized and lie close together in energy. The electron is able to nonadiabatically cascade through these closely spaced levels with a very high rate until it reaches the lowest excited state. If the gap between this excited state and the ground state is small, the electron can continue its cascade and radiationlessly enter the ground state, where it can undergo rapid self-trapping and reach equilibrium. For slightly larger initial gaps the electron remains in the first excited state, resulting in the two qualitatively different types of trajectories. In these latter examples, the ground and first excited states pair off and at early times manifest an energy separation of ~ 0.2 eV.[31] This separation is about 1/3 that of the equilibrium excited state gap produced after photoexcitation, so the computed excited state lifetime after injection of ~ 160 fs correlates well with a roughly linear gap dependence of the nonadiabatic transition rate given the ~ 450 fs lifetime computed here. In other words, we conclude that the solvent response is slow enough that in the injection case, the small initial energy gap leads to radiationless decay before the excited state can undergo equilibration. In the photoexcitation case, the additional slowing of the decay due to excited state solvation dynamics further contributes to the large difference in relaxation time scales between the two experiments. Thus, the evolution of local solvent configurations, starting from either neat water in the case of electron injection or the equilibrium hydrated electron in the case of photoexcitation, result in different evolution of the quantum energy gap which is ultimately responsible for the difference in relaxation physics observed in both simulation and experiment.

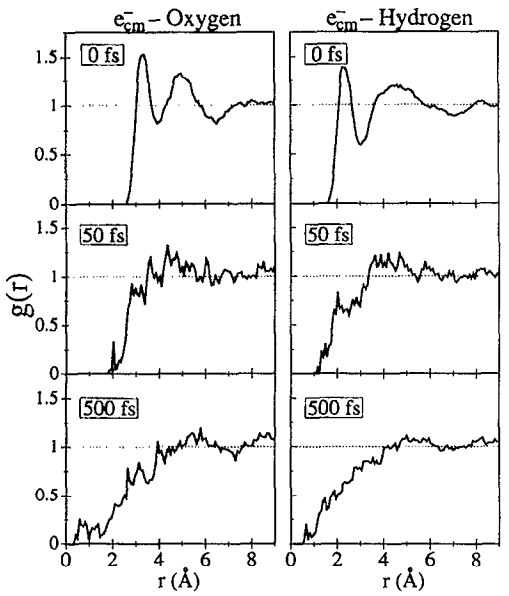

FIG. 7. Time-dependent center of mass–solvent atom pair distribution functions for the hydrated electron following photoexcitation. The upper plots give the solvent structure at the instant of photoexcitation: they are identical to the equilibrium structure of the hydrated electron. The center plots show the average pair distributions 50 fs after photoexcitation, showing the solvent structure after completion of the inertial solvent response. The lower plots show the average solvent structure of the equilibrium excited state which occurs 500 fs following promotion.

B. Microscopic solvation structure

As discussed in Sec. I, electrons in aqueous solution are self-trapped; they become localized in a solvent cavity which is about the size of a Br^- ion. If this cavity were perfectly spherical, the first three excited states would be p-like in character and triply degenerate. Instead, deviations from spherical symmetry lift this degeneracy and causing a splitting of the three p-like states by nearly 0.8 eV (see Fig. 1).[23] Size fluctuations of the cavity correlate with changes in the average excited state energy, while cavity shape changes modulate the splitting between the states.[20] From simple considerations of the behavior of a particle in a box, the lowest energy state has its nodal plane perpendicular to the long principle axis of the distorted cavity, while the highest energy state is aligned along the short principle axis. Since the resonance condition used in these simulations lies near the red edge of the absorption band (Fig. 1), most of the excitation is along the long axis of the cavity, to the lowest excited state.

To better understand the structure of the solvent cavity containing the hydrated electron and the changes it undergoes upon excitation, we have computed time-dependent electron-solvent radial distribution functions. We have chosen the electron center of mass as the common origin for all the pair distribution functions, which are displayed in Fig. 7. The upper two plots in Fig. 7 display the electron–hydrogen $[g_{e^-\text{-}H}(r)]$ and electron–oxygen $[g_{e^-\text{-}O}(r)]$ radial distribution functions at the time of excitation. Since the electrons are excited from equilibrium, these are also the ground state equilibrium pair distribution functions. These traces were ensemble averaged over the ground state configurations for 250 fs prior to excitation (5000 configurations total), and agree well with previous calculations. Previous work using the same pseudopotential but a rigid model for water found very similar results,[22] indicating that molecular flexibility has little effect on the equilibrium hydration structure of the solvated electron.

In order to clarify the time evolution after excitation, we pause to comment on the equilibrium structure of the hydrated electron. The upper plots of Fig. 7 show that the negatively charged O atoms are repelled from the electron and lie on a sphere just outside most of the electronic charge density. The first solvation shell for the positively charged H atoms lies ~1 Å, or one O–H bond length, closer to the electron center of mass, indicative of radial alignment of the O–H bonds. For both the H and O pair distributions, the positions of the peaks are similar to that of an ion of similar size such as Br^- or Cl^-, but the peak amplitudes are significantly smaller. This is a manifestation of the size and shape fluctuations of the hydrated electron, which smear out the sharpness of the local solvent structure.[20,22] This relatively weak imposition of solvent ordering by the solute has other ramifications for the local structure. Previous calculations have suggested that the water–water correlations in the vicinity of the hydrated electron are not significantly perturbed from the bulk,[22] a result in agreement with the small solvation entropy of electron hydration.[72,73] The fact that the solvation structure around the hydrated electron is not critically different from that of neat water most likely plays a large role in the linear solvation response upon photoexcitation.

To investigate the changes in solvation structure associated with different portions of the solvation response, we have also computed radial distribution functions for the hydrated electron at delays of 50 and 500 fs after photoexcitation. The center plots in Fig. 7 display $g_{e^-\text{-}H}(r)$ and $g_{e^-\text{-}O}(r)$ averaged over the 19 trajectories in which the electron occupied the excited state between 25 and 75 fs after photoexcitation (950 configurations total). While these traces are somewhat noisier than the equilibrium pair distributions due to the lower number of averaged configurations, they do show the changes in solvent structure associated with completion of the inertial component of the solvation response.

The most striking feature of the center plots in Fig. 7 is the essentially complete destruction of the local solvent structure after only 50 fs; the pair distribution functions are nearly featureless. In addition, the turn-on points for the distributions have moved significantly inward (~0.5 Å) during this same time period. This is a direct result of the shape change of the electron upon excitation. Radially oriented water molecules along the short axis of the aspherical cavity, which were already slightly closer to the electron's center of mass before the excitation, find themselves aligned along the nodal plane in the electronic wave function after promotion to the p-like excited state. Mechanical pressure of the second solvation shell directs these molecules toward the newly created void, so that the translational and rotational inertial motion of these molecules causes them to coast into the nodal region, bringing them even closer the electron's center of

mass. The strong Coulombic attraction between the two lobes of the electronic charge distribution and the positively charged H atoms entering the nodal region may assist this process, and probably accounts for much of the change in solvation energy which occurs over this short time. Small bumps in the pair distributions, which appear to be remnants of the equilibrium first and second solvent shells, mirror this inward moving trend.

This signature points to the importance of low-frequency translational motions in the coupling to the solvent response. Phononlike motions of water molecules causing net translation in toward the electron center of mass (e.g., the H-bond stretch and bending motions near 170 and 65 cm^{-1}, respectively)[74] seem to play a critical role in the solvation dynamics. The Fourier transform of the solvent response function presented in Fig. 6 shows large features at these low frequencies and almost no contributions from intramolecular modes, indicating the importance of low frequency translational motions in the solvent response. The strength of this coupling can also be seen in the contributions to the computed ultrafast spectroscopy,[26,37] where strong oscillations in the 50–150 cm^{-1} range can be seen. This idea is also in accord with the conclusions of instantaneous normal mode (INM) analysis for molecular liquids.[75–77] The solvent INMs coupled to the solute show a strong degree of translational character, and for water, this distribution peaks around 100 cm^{-1}.[78,79]

Once the inertial solvation dynamics are complete, the collective response of the solvent to the new charge distribution leads to further changes in the local structure. The lower plots of Fig. 7 show electron–solvent pair distribution functions ~500 fs after photoexcitation. These essentially represent the equilibrium structure of the excited state. The results are the ensemble average over the 13 trajectories in which the electron resides in the excited state between 450 and 550 fs after photoexcitation (1300 configurations total). These plots show that the structural trends initiated during the first 50 fs following promotion have continued. The initial rise for both distributions has moved inwards toward zero, as water molecules have diffused into the nodal region close to the center of mass. Molecules that were along the long axis of the equilibrium cavity, and hence, initially farther from the center of mass, are further repelled from the center of mass after excitation places them within the repulsive region of the pseudopotential (mechanical response). This solvent diffusion away from the center of mass, combined with motion inwards along the nodal plane leads to the smooth, featureless average radial distribution.

Since the excited state of the hydrated electron is more cylindrical than spherical, the radial pair distribution functions are not the best way to explore the details of the local solvent structure. One way to better examine the shape of the cavity after excitation is to construct pair distribution functions which take advantage of the approximate local cylindrical symmetry. Introducing a set of cylindrical coordinates with the electron center of mass at the origin and the z axis running along the long principal axis of the solvent cavity (see below), we can define the two-dimensional cylindrical pair distribution functions $g^{A}_{cyl}(r,z)$ by

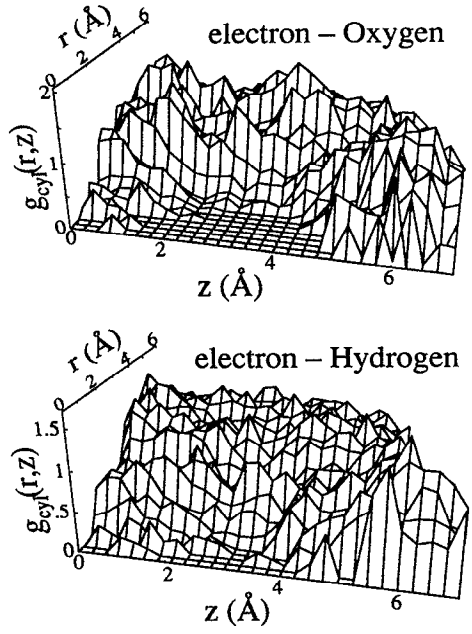

FIG. 8. Two-dimensional cylindrical pair distribution functions for the equilibrated excited state hydrated electron (times ≥1 ps), calculated by Eq. (7). The origin denotes the electron center of mass and the z axis lies along the transition dipole vector connecting the occupied and ground states. See the text for details.

$$2\pi\rho g^{A}_{cyl}(r,z)=\left\langle \frac{1}{N}\sum_{i=1}^{N}\delta(r-r_i^A)\,\delta(z'-z_i^A+z_{cm})\right\rangle, \tag{7}$$

where the sum runs over the N members of atomic species A (either H or O), the subscript cm denotes the electron center of mass position, ρ is the solvent density, $z=|z'-z_{cm}|$ is the distance along the cavity z axis from the center of mass, and r is the radial (polar) distance from the z axis. This function essentially provides a polar equivalent to $g(r)$ for different values of z along the long principal axis of the solvent cavity, averaged azimuthally around the z axis and over the two possible ways of being distance z from the center of mass. Unlike the one-dimensional radial distribution function which uses assumed spherical symmetry to average over the two spherical-polar angles, the two-dimensional cylindrical pair distribution functions of Eq. (7) are integrated only over the one azimuthal coordinate and averaged over $\pm z$. Thus, the extra information present in the two-dimensional $g^{A}_{cyl}(r,z)$ is partially offset by the large decrease in counting statistics due to integration over a fewer total number of degrees of freedom.

Figure 8 displays the cylindrical pair distribution functions for the equilibrated excited state hydrated electron calculated via Eq. (7). To define the coordinate system, we recall that excitation to the lowest excited state places the node of the excited wave function perpendicular to the long axis of the distorted solvent cavity. Since the transition dipole matrix element vector connecting the ground and first excited states also lies perpendicular to the node in the excited (occupied) wave function, it parallels the direction of the

long principal axis of the cavity. This allows a cylindrical coordinate system to be defined for each individual configuration: the origin lies at the electron center of mass, and the z axis points along $\langle \Psi_{gnd}(t)|\mathbf{r}|\Psi_{occ}(t)\rangle$. The two plots of Fig. 8 represent the ensemble average over all times $\geq$1000 fs in which the electron occupies the excited state (~6500 total configurations); as expected, the plots show considerable noise compared to the spherically averaged $g(r)$'s displayed in Fig. 7. Despite these statistics, Fig. 8 clearly reveals the solvent structure of the equilibrium excited state of the hydrated electron.

The upper plot in Fig. 8 shows the e^-–O cylindrical pair distribution function. Like the $g_{e^-\text{-}O}(r)$ presented in Fig. 7, the excluded region defines the shape of the local solvent cavity. The solvent oxygen atoms are expelled from a peanut-shaped cavity, which can be readily visualized by rotating the excluded region in the Fig. 8 around the z axis and reflecting about the origin (center of mass). The electron occupies the axial region from 0 to 4.5 Å along the z axis (9 Å in total length), but only extends ~2 Å radially into the solvent at its point of widest extent. Thus, the solvent cavity has completely rearranged to accommodate the p-like shape of the excited hydrated electron, which since promotion has grown by a factor of ~2 along the cavity long axis while remaining mostly unchanged in diameter in the other two directions. The cavity is sharply defined at the axial maxima of the p-like lobes along the z axis, but appears more smeared in the nodal region near $z=0$ Å and in the region of largest radial diameter around $z=3$ Å. This is likely a consequence of the large fluctuations in size and shape of the hydrated electron.

The lower portion of Fig. 8 displays the cylindrical e^-–H pair distribution function. Comparison of the two plots in Fig. 8 reveals that many of the general features in the e^-–O $g_{cyl}(r,z)$ are also present in the e^-–H $g_{cyl}(r,z)$, but at radial distances roughly one O–H bond length (~1 Å) smaller, indicating a tendency for polar alignment of the water molecules around the excited state electron.

Unfortunately, our attempts to extract dynamical solvent structural information by computing time-dependent cylindrical pair distributions in the manner of Fig. 7 were hampered by poor statistics. An alternate way to examine the shape of the solvent cavity following excitation is to use the wave function of the electron itself to track the cavity. While the wave function of the excited state electron is p-like and has a node, the (unoccupied) ground state adiabatic eigenfunction does not and readily reveals the general shape of the surroundings. Figure 9 displays the unoccupied ground state eigenfunctions for the electron at different times after excitation for the trajectory shown in Fig. 2. The plots of Fig. 9 are two-dimensional cuts through the three-dimensional electronic wave function (not angle averages), where the plane of the cut is chosen to contain the electron center of mass and the transition dipole matrix vector connecting the ground and first excited states. Thus, for the trajectory shown, the slices presented in Fig. 9 are oriented so as to intersect the previously defined long axis of the cavity; however, the absolute orientation of the plane shown remains fixed in the lab frame.

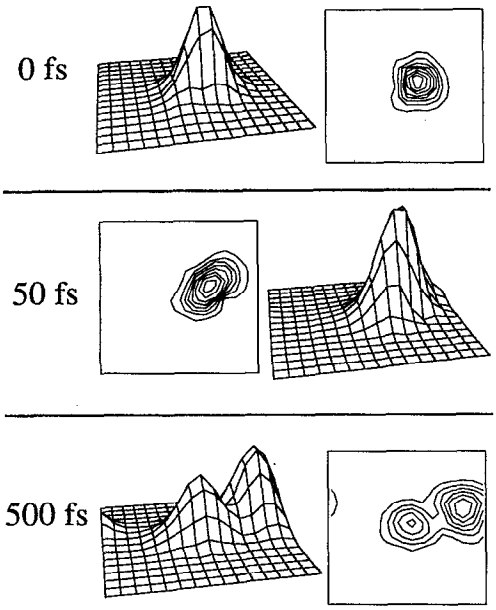

FIG. 9. Selected ground state eigenfunctions, shown in perspective and as contour plots, at various time delays for the trajectory shown in Fig. 2 demonstrating dynamic evolution of the solvent cavity containing the electron following photoexcitation. The plane of these two-dimensional slices contains both the electron center of mass and the transition dipole vector connecting the ground and occupied excited states. See the text for details.

The upper portion of Fig. 9 shows the electronic wave function at the instant of excitation. The wave function looks fairly symmetric, and the contour plot shows only a small deviation from spherical symmetry along the long axis of the cavity, which makes a roughly 45° angle with the edges of the box. By 50 fs after promotion to the excited state, shown in the center section of Fig. 9, the solvent cavity has undergone significant distortion along the long axis of the cavity: the electron has become nearly 50% longer, and there is evidence for solvent molecules moving in towards the center of mass near the nodal plane, as seen in the indentation in the lower right-hand portion of the contour plot. These distortions in both the shape and size of the cavity are strictly the result of inertial motions of the solvent molecules following excitation. When the solvent response is complete and the electron has reached equilibrium in the excited state, the solvent cavity takes on its overall peanut shape, seen 500 fs after excitation in the lower portion of Fig. 9. The electron has now roughly doubled in size along the original long axis of the cavity.

It is interesting to note that while size of the electron along the cavity long axis changes significantly with time, Fig. 9 shows that the orientation of the long axis remains relatively constant with time. Even 500 fs after photoexcitation, the long cavity axis has rotated at most 15° from its initial direction. This decoupling of the solvent fluctuations distorting the size and orientation of the cavity keeps the three p-like excited states from rapidly interchanging roles as defined by a direction in space. This can be seen by examining the autocorrelation function of the transition dipole vectors, which point along the cavity principle axes. Previous calculations have found that the transition dipole corre-

lations decay biphasically, with time scales of ~0.25 and ~1 ps.[36] The longer of these time scales for long axis reorientation is comparable to the excited state residence time of the hydrated electron. This opens the possibility of detecting polarized fluorescence or using polarized transient hole burning as a means of spectroscopically separating the time scales of these isotropic and anisotropic components of the solvent fluctuations. Detailed predictions for the results of polarized transient hole-burning experiments based on the simulations discussed here have been presented in a previous report,[37] and experiments along these lines have recently been completed.[80]

The large change in size and shape of the electron upon photoexcitation raises the possibility that much of the solvent response may be mechanical rather than dielectric in nature. Recent experimental[81,82] and theoretical[83–85] studies of nonpolar solvation dynamics have shown that a mechanical perturbation produces a time-dependent solvation response similar to that presented in Fig. 6. A simple model treating the solvent as a visco-elastic continuum[83] is able to reproduce much of these dynamics,[81,82] indicating that the mechanical stress and strain responses of the solvent play an important role in solvation dynamics. We have found that the solvation response following photoexcitation of the electron (Fig. 6) is significantly different from that following the nonadiabatic transition back to the ground state. Since the electron grows by a factor of ~2 upon photoexcitation and shrinks by the same amount upon radiationless relaxation, the differences are most likely due to the mechanical response of the solvent. Upon photoexcitation, the electron is strongly expanding along the z axis while a potential void is formed along the x–y plane, creating an anisotropic stress on the surrounding solvent which leads to mechanical relaxation that requires translational rearrangement of the solvent molecules. Upon radiationless decay, the electron contracts leaving a void which is readily filled by the solvent. This issue of the interplay between mechanical and electrical contributions to solvation dynamics will be the subject of a forthcoming publication.[70]

Overall, the information of Figs. 7–9 provides a qualitative understanding of the microscopic changes associated with the solvent response depicted in Figs. 4 and 6. At equilibrium, the hydrated electron occupies an s-like state in a slightly aspherical solvent cavity. The deviation from spherical symmetry splits the first three excited states, and solvent fluctuations which change the size and shape of the cavity modulate the adiabatic eigenstates of the solute. Photoexcitation on the red edge of this band of three p-like states promotes the electron into the lowest excited state which is oriented along the long principle axis of the cavity. The solvent responds rapidly to this change in charge distribution, moving to create a peanut-shaped cavity and allowing the electron to become larger in size along the long cavity axis. The O–H bonds of the first few solvent shells which had been radially aligned from the electron center of mass reorient to become aligned in a polar manner due to the cylindrical symmetry of the excited electron. The potential energy released by this solvent reorientation is fortuitously offset by the decrease in kinetic energy as the electron becomes larger (less curvature to the wave function), causing little net energy change of the occupied state. The change in cavity shape, however, strongly affects the energies of the other adiabatic eigenstates. The formerly s-like ground state is now forced to significantly distort in order to fit inside the expanding peanut-shaped cavity, causing its energy to increase in direct proportion to the solvation response. The upper two p-like states, which had been aligned along the other two principle cavity axes oriented perpendicularly to the occupied wave function, must also distort to avoid the solvent molecules which have drifted into the nodal region of the occupied state, raising their energy. The continuum states, which are delocalized over the entire simulation box are largely unaffected by these local cavity changes so their energy remains mostly unchanged. Since the solvent response to the change in charge distribution upon photoexcitation is linear, we expect that many of these ideas about the details of the relationship between solvent response and solute size and shape should hold generally for the case of aqueous solvation dynamics, and possibly for solvation dynamics in general.

V. CONCLUSIONS

In summary, we have used computer simulation to examine the nature of solvation dynamics in aqueous solution using a realistic quantum mechanical solute, the hydrated electron. The electron is described at the Hamiltonian level, so the extended charge distribution and polarizability of the solute are treated explicitly, and a prescription for molecular dynamics with electronic transitions is employed. In this way, the effects of solvation dynamics on quantum eigenstates can be studied in detail, and quantum eigenfunctions can be used to compute ultrafast spectroscopic transients for direct comparison to experiment.

Individual nonadiabatic trajectories simulating photoexcitation of the electron show strong modulation of the electronic eigenstates by solvent fluctuations and a large decrease of the energy gap upon solvation. The solvent response is characterized by a 25 fs Gaussian inertial component superimposed on a 250 fs exponential decay. Both the time dependence and absolute magnitude of the solvation response indicate that solvent relaxation for photoexcitation of the hydrated electron falls in the linear regime, despite the enormously large 75% fractional Stokes' shift.

An examination of microscopic solvent structural changes following photoexcitation of the electron shows that low frequency translational motions are important to the solvation response. Water molecules are driven both mechanically and electrostatically into the nodal region of the hydrated electron as well as away from the axial extremes of the p-like lobes of the excited state charge distribution. The importance of solvent translational motion and the possible interplay between mechanical and dielectric solvent responses have received little attention in the solvation dynamics literature, but are clearly important for the case of the hydrated electron as evidenced in the relatively small (40%) amplitude of the inertial component of the solvent response.

Reorientational motion of water molecules accommodating the excited state charge distribution of the electron is also important in the dielectric response. Much of the solvation

dynamics may be driven by the large change in shape of the electron during the solvent response. Radially aligned electron–water hydrogen bonds which characterize the ground state of the electron become aligned around the approximately cylindrically symmetric excited state species. The excited state electron grows by a factor of about 2 along the symmetry axis while maintaining its original average size in the other two dimensions. This growth of the electron lowers its kinetic energy, explaining why little of the solvation response is manifest in the excited state energy and reemphasizing the importance of a realistic quantum description for the solute in studies of solvation dynamics.

The large change in the quantum energy gap driven by solvent relaxation plays an important role in the radiationless relaxation of the hydrated electron. A simple model assuming that the nonradiative transition probability is inversely proportional to the quantum energy gap is able to reproduce the general features of the observed survival probability. If this idea holds generally, then it should be possible to significantly increase the excited state residence time of a solvated electron by choosing experimental conditions where the solvation response is very slow so that the energy gap remains large. In this way, it may be possible to observe long-lived absorption transients or even fluorescence from electrons trapped in slow-moving fluids such as low temperature alcohols.

The gap-dependent nonradiative rate can also explain the differences between electron photoinjection and photoexcitation experiments. In the photoinjection case, the quantum eigenstates start together in a band, and only begin to separate as solvation of the electron proceeds. Since the energy gaps are initially small, the radiationless transition rate is relatively high, so electrons undergo a rapid nonadiabatic cascade to the ground or first excited state. Even for those electrons trapped in the first excited state, the nascent gap to the ground state is initially small enough for these electrons to undergo radiationless relaxation to the ground state before excited state solvation proceeds to any appreciable extent. In the photoexcitation case, however, the initial quantum gap is large, and rapid radiationless decay can only occur after the solvation dynamics are complete, leading to an excited state residence time which is a factor of ~ 5 longer than in the photoinjection case. It is gratifying that the physics observed in both types of experiments are well reproduced by a single model for the hydrated electron.

Overall, the richness of information presented here leads to the tentative suggestion that electrons could serve as a "universal" probe of solvation dynamics. Electrons are soluble in a wide variety of polar and nonpolar solvents and have reasonably large optical cross sections in the visible and near infrared. The electronic eigenstates are strongly coupled to solvent fluctuations, and there is no complicating internal vibrational or rotational structure. But perhaps most importantly, electrons are amenable to a high level of theory, reinforcing the close connection being made between solvation dynamics, ultrafast spectroscopy, and molecular dynamics simulations.

ACKNOWLEDGMENTS

This work was supported by the National Science Foundation. We acknowledge Paul Barbara for generously sharing results and ideas prior to publication. B. J. S. thanks Sandy Rosenthal, Wayne Bosma, Phil Reid, and Ed Castner for many stimulating discussions. One of the authors (B.J.S.) gratefully acknowledges the support of NSF Postdoctoral Research Fellowship Grant No. CHE-9301479 awarded in 1993, and the allocation of computational resources from the San Diego Supercomputing Center.

[1] *Water, a Comprehensive Treatise*, edited by F. Franks (Plenum, New York, 1982).
[2] M. Maroncelli, J. Mol. Liq. **57**, 1 (1993).
[3] P. F. Barbara and W. Jarzeba, Adv. Photochem. **15**, 1 (1990).
[4] See, e.g., P. J. Reid, C. Silva, P. F. Barbara, L. Karki, and J. T. Hupp, J. Chem. Phys. (submitted).
[5] Y. J. Chang and E. W. Castner, J. Chem. Phys. **99**, 7289 (1993).
[6] Y. J. Chang and E. W. Castner, J. Chem. Phys. **99**, 113 (1993).
[7] N. F. Scherer, M. Cho, L. D. Ziegler, M. Du, A. Matro, J. Cina, and G. R. Fleming, in *Ultrafast Phenomenon VIII*, edited by J.-L. Martin, A. Migus, G. A. Mourou, and A. H. Zewail Springer Series in Chemical Physics, Vol. 55 (Springer, New York, 1993), p. 99.
[8] R. J. D. Miller, J. Deak, S. Palese, M. Pereira, L. Richard and L. Schlling, in Ref. 7, p. 525.
[9] W. Jarzeba, G. C. Walker, A. E. Johnson, M. A. Kahlow, and P. F. Barbara, J. Phys. Chem. **92**, 7039 (1988).
[10] G. C. Walker, W. Jarzeba, A. E. Johnson, and P. F. Barbara, J. Opt. Soc. Am. B **7**, 1521 (1990).
[11] R. Jimenez, G. R. Fleming, K. Papazyan, and M. Maroncelli, Nature **369**, 471 (1994).
[12] M. Maroncelli and G. R. Fleming, J. Chem. Phys. **89**, 5044 (1988).
[13] O. A. Karim, A. D. J. Haymet, M. J. Banet, and J. D. Simon, J. Phys. Chem. **92**, 3391 (1988).
[14] J.-K. Hwang, G. King, S. Creighton, and A. Warshel, J. Am. Chem. Soc. **110**, 5297 (1988).
[15] R. M. Levy, D. B. Kitchen, J. T. Blair, and K. Krogh-Jespersen, J. Phys. Chem. **94**, 4470 (1990).
[16] P. L. Muiño and P. R. Callis, J. Chem. Phys. **100**, 4093 (1994).
[17] J. S. Bader and D. Chandler, Chem. Phys. Lett. **157**, 501 (1990).
[18] R. B. Barnett, U. Landman, and A. Nitzan, J. Chem. Phys. **90**, 4413 (1989).
[19] S. Roy and B. Bagchi, J. Chem. Phys. **99**, 9938 (1993).
[20] P. J. Rossky and J. Schnitker, J. Phys. Chem. **92**, 4277 (1988).
[21] See, e.g. K. A. Motakabbir, J. Schnitker, and P. J. Rossky, J. Chem. Phys. **97**, 2055 (1992).
[22] J. Schnitker and P. J. Rossky, J. Chem. Phys. **86**, 3471 (1987).
[23] J. Schnitker, K. Motakabbir, P. J. Rossky, and R. A. Friesner, Phys. Rev. Lett. **60**, 456 (1988).
[24] J. C. Alfano, P. K. Walhout, Y. Kimura, and P. F. Barbara, J. Chem. Phys. **98**, 5996 (1993).
[25] Y. Kimura, J. C. Alfano, P. K. Walhout, and P. F. Barbara, J. Phys. Chem. **98**, 3450 (1994).
[26] B. J. Schwartz and P. J. Rossky, J. Phys. Chem. **98**, 4489 (1994).
[27] A. Migus, Y. Gauduel, J. L. Martin, and A. Antonetti, Phys. Rev. Lett. **58**, 1559 (1987).
[28] F. H. Long, H. Lu, and K. B. Eisenthal, Phys. Rev. Lett. **64**, 1469 (1990).
[29] S. Pommeret, A. Antonetti, and Y. Gauduel, J. Am. Chem. Soc. **113**, 9105 (1991).
[30] F. H. Long, H. Lu, X. Shi, and K. B. Eisenthal, Chem. Phys. Lett. **185**, 47 (1991).
[31] T. H. Murphrey and P. J. Rossky, J. Chem. Phys. **99**, 515 (1993).
[32] F. A. Webster, J. Schnitker, M. S. Friedrichs, R. A. Friesner, and P. J. Rossky, Phys. Rev. Lett. **66**, 3172 (1991).
[33] E. Keszei, T. H. Murphrey, and P. J. Rossky, J. Phys. Chem. (submitted).
[34] E. Keszei, S. Nagy, T. H. Murphrey, and P. J. Rossky, J. Chem. Phys. **99**, 2004 (1993).
[35] J. Schnitker and P. J. Rossky, J. Chem. Phys. **86**, 3462 (1987).
[36] K. A. Motakabbir, J. Schnitker, and P. J. Rossky, J. Chem. Phys. **90**, 6916 (1989).
[37] B. J. Schwartz and P. J. Rossky, Phys. Rev. Lett. **72**, 3282 (1994).

[38] P. J. Rossky, J. Opt. Soc. Am. B **7**, 1727 (1990).
[39] E. J. Hart and J. W. Boag, J. Am. Chem. Soc. **84**, 4090 (1962).
[40] See, e.g., F.-Y. Jou and G. R. Freeman, J. Phys. Chem. **83**, 2383 (1979).
[41] K. Toukan and A. Rahman, Phys. Rev. B **31**, 2643 (1985).
[42] H. J. C. Berendsen, J. P. M. Postma, W. F. van Gunsteren, and J. Hermans, in *Intermolecular Forces*, edited by B. Pullman (Reidel, Dordrecht, 1981), p. 331.
[43] K. Watanabe and M. L. Klein, Chem. Phys. **131**, 157 (1989).
[44] J.-L. Barrat and I. R. McDonald, Mol. Phys. **70**, 535 (1990).
[45] A. Wallqvist and O. Teleman, Mol. Phys. **74**, 515 (1991).
[46] D. F. Coker, in *Computer Simulations in Chemical Physics*, edited by M. P. Allen and D. J. Tildesley (Kluwer Academic, Dordrecht, 1993), p. 315.
[47] F. A. Webster, P. J. Rossky, and R. A. Friesner, Comput. Phys. Commun. **63**, 494 (1991).
[48] F. Webster, E. T. Wang, P. J. Rossky, and R. A. Friesner, J. Chem. Phys. **100**, 4835 (1994).
[49] J. C. Tully and R. K. Preston, J. Chem. Phys. **55**, 562 (1971).
[50] P. Pechukas, Phys. Rev. **181**, 174 (1969).
[51] B. Space and D. F. Coker, J. Chem. Phys. **94**, 1976 (1991).
[52] B. Space and D. F. Coker, J. Chem. Phys. **96**, 652 (1992).
[53] J. C. Tully, J. Chem. Phys. **93**, 1061 (1990).
[54] E. Neria, A. Nitzan, R. N. Barnett, and U. Landman, Phys. Rev. Lett. **67**, 1011 (1991).
[55] E. Neria and A. Nitzan, J. Chem. Phys. **99**, 1109 (1993).
[56] D. F. Coker, J. Chem. Phys. (submitted).
[57] See, e.g., M. P. Allen and D. J. Tildesley, *Computer Simulation of Liquids* (Oxford University Press, New York, 1987).
[58] Note that the calculated ground state absorption spectrum is ~0.7 eV blue-shifted from experiment, as seen in Ref. 23. This simple linear frequency shift for the pump and probe wavelengths gives excellent agreement between calculated and experimental transients in the visible and near IR regions, but clearly cannot apply at the extreme wavelengths, for example, the equilibrium excited state gap of 0.56 eV. We expect that the fractional Stokes shift quoted in the text will make a better comparison to experiment.
[59] See, e.g., G. van der Zwan and J. T. Hynes, J. Phys. Chem. **89**, 4181 (1985).
[60] See, e.g., D. McMorrow and W. T. Lotshaw, Chem. Phys. Lett. **174**, 85 (1990).
[61] M. Maroncelli, P. V. Kumar, A. Papazyan, M. L. Horng, S. J. Rosenthal, and G. R. Fleming, in *Ultrafast Reaction Dynamics and Solvent Effects*, edited by Y. Gauduel and P. J. Rossky [AIP Conf. Proc. **298**, 310 (1994)].
[62] B. Bagchi and A. Chandra, J. Chem. Phys. **97**, 5126 (1992).
[63] A. Chandra, D. Wei, and G. N. Patey, J. Chem. Phys. **99**, 4926 (1993).
[64] F. O. Raineri, H. Resat, B. C. Perng, F. Hirata, and H. L. Friedman, J. Chem. Phys. **100**, 1477 (1994).
[65] S. J. Rosenthal, X. Xie, M. Du, and G. R. Fleming, J. Chem. Phys. **95**, 4715, (1991).
[66] S. J. Rosenthal, N. F. Scherer, M. Cho, X. Xie, M. E. Schmidt and G. R. Fleming, in Ref. 7, p. 616.
[67] S. J. Rosenthal, R. Jimenez, G. R. Fleming, K. Papazayan, and M. Maroncelli, J. Mol. Liq. (in press).
[68] M. Maroncelli, V. P. Kumar, and A. Papazyan, J. Phys. Chem. **97**, 13 (1993).
[69] P. V. Kumar and M. Maroncelli, (unpublished).
[70] B. J. Schwartz and P. J. Rossky, J. Chem. Phys. (unpublished).
[71] This relation is valid in the high temperature limit. See, e.g., Y. J. Yan and S. Mukamel, J. Chem. Phys. **89**, 5160 (1988).
[72] B. C. Webster, Annu. Rep. Prog. Chem. Sect. C **76**, 287 (1979).
[73] J. Jortner and R. M. Noyes, J. Phys. Chem. **70**, 770 (1966).
[74] See, e.g. G. E. Walrafen, J. Phys. Chem. **94**, 2237 (1990).
[75] M. Buchner, B. M. Landanyi, and R. M. Stratt, J. Chem. Phys. **97**, 8522 (1992).
[76] T.-M. Wu and R. F. Loring, J. Chem. Phys. **99**, 8936 (1993).
[77] R. M. Stratt and M. Cho, J. Chem. Phys. **100**, 6700 (1994).
[78] M. Cho, G. R. Fleming, S. Saito, I. Ohmine, and R. M. Stratt, J. Chem. Phys. **100**, 6672 (1994).
[79] S. Sastry, H. E. Stanley, and F. Sciortino, J. Chem. Phys. **100**, 5361 (1994).
[80] P. J. Reid, C. Silva, P. K. Walhout, and P. F. Barbara, Chem. Phys. Lett. (in press).
[81] J. T. Fourkas, A. Benigno, and M. Berg, J. Chem. Phys. **99**, 8552 (1993).
[82] J. T. Fourkas and M. Berg, J. Chem. Phys. **98**, 7773 (1993).
[83] M. Berg (private communication).
[84] B. Bagchi, J. Chem. Phys. **100**, 6658 (1994).
[85] A. Chandra and B. Bagchi, J. Chem. Phys. **99**, 553 (1993).